The LeuT-fold neurotransmitter:sodium symporter MhsT has two substrate sites

Matthias Quick[a,b,c,1], Ara M. Abramyan[d], Pattama Wiriyasermkul[a], Harel Weinstein[e], Lei Shi[d], and Jonathan A. Javitch[a,b,c,f,1]

[a]Department of Psychiatry, Columbia University College of Physicians and Surgeons, New York, NY 10032; [b]Center for Molecular Recognition, Columbia University College of Physicians and Surgeons, New York, NY 10032; [c]Division of Molecular Therapeutics, New York State Psychiatric Institute, New York, NY 10032; [d]Computational Chemistry and Molecular Biophysics Unit, Molecular Targets and Medications Discovery Branch, NIH/National Institute on Drug Abuse/Intramural Research Program, Baltimore, MD 21224; [e]Department of Physiology and Biophysics and Institute for Computational Biomedicine, Weill Cornell Medical College of Cornell University, New York, NY 10065; and [f]Department of Pharmacology, Columbia University College of Physicians and Surgeons, New York, NY 10032

Edited by Ernest M. Wright, David Geffen School of Medicine at UCLA, Los Angeles, CA, and approved July 13, 2018 (received for review October 5, 2017)

Crystal structures of the neurotransmitter:sodium symporter MhsT revealed occluded inward-facing states with one substrate (Trp) bound in the primary substrate (S1) site and a collapsed extracellular vestibule, which in LeuT contains the second substrate (S2) site. In *n*-dodecyl-β-D-maltoside, the detergent used to prepare MhsT for crystallization, the substrate-to-protein binding stoichiometry was determined by using scintillation proximity to be 1 Trp:MhsT. Here, using the same experimental approach, as well as equilibrium dialysis, we report that in *n*-decyl-β-D-maltoside, or after reconstitution in lipid, MhsT, like LeuT, can simultaneously bind two Trp substrate molecules. Trp binding to the S2 site sterically blocks access to a substituted Cys at position 33 in the S2 site, as well as access to the deeper S1 site. Mutation of either the S1 or S2 site disrupts transport, consistent with previous studies in LeuT showing that substrate binding to the S2 site is an essential component of the transport mechanism.

membrane transport | neurotransmitter:sodium symporter | LeuT fold | MhsT

Neurotransmitter:sodium symporters (NSSs) terminate chemical neurotransmission through the reuptake of released neurotransmitters via a symport process driven by the movement of Na^+ down its concentration gradient (1, 2). Biogenic amine NSS (members of the SLC6 family), including transporters for serotonin, norepinephrine, and dopamine have gained particular attention as they have been implicated in disorders such as depression (3) and autism (4) and are the molecular targets of antidepressant drugs [including selective serotonin reuptake inhibitors (SSRIs) and tricyclic antidepressants (TCAs)], as well as of therapeutic and illicit psychostimulants, such as amphetamine and cocaine (5, 6). Functional studies have revealed key mechanistic features of these transporters (7–10), but structural information for the NSS family was not available until 2005 when LeuT, a bacterial NSS homolog, was crystallized (11). The LeuT structure [Protein Data Bank (PDB) ID code 2A65] features an occluded binding pocket with one leucine in the centrally located primary substrate (S1) binding site and Na^+ in two Na^+ sites (termed Na1 and Na2) (11). LeuT shares a structural fold (the so-called LeuT fold) with three subsequently crystallized NSS members, the multihydrophobic substrate transporter MhsT from *Bacillus halodurans* (12, 13), the *Drosophila* dopamine transporter, dDAT (14–16), and the human serotonin transporter, hSERT (17). In addition, other transporter families have also been shown to share the LeuT fold despite a lack of primary sequence conservation (18, 19).

Our computational and biochemical studies on LeuT revealed the existence of a second substrate (S2) binding site, located above the S1 site in the extracellular vestibule (20), and we proposed a mechanistic model in which allosteric interactions between the S1 and S2 sites regulate Na^+-coupled substrate symport (20, 21). Consistent with this model, using LeuT reconstituted into lipid nanodiscs, an independent study reported a substrate-to-LeuT binding stoichiometry of ∼2 for Leu and Ala (22). Nonetheless, the existence of a high-affinity S2 site for substrate has been challenged (23, 24), in part due to the lack of a LeuT crystal structure with a substrate-occupied S2 site. However, several reports highlight the interaction of the S2 site with TCAs, SSRIs, or detergents used in the preparation of LeuT for crystallographic studies (25–29) (*SI Appendix*, Fig. S1). Importantly, raising the concentration of the detergent *n*-dodecyl-β-D-maltopyranoside (DDM) abolishes substrate binding to the S2 site (29), and computational simulations have shown that at these concentrations DDM penetrates into the S2 site where it remains bound (30). Substrate binding to the S2 site is restored by reconstitution into proteoliposomes, demonstrating the functionality of the site in the native lipid environment (29). Interestingly, the recent crystal structure of hSERT that features S-citalopram bound not only in the S1 site, but also in a second site in the extracellular vestibule (*SI Appendix*, Fig. S1), adds additional support for the existence of two binding sites in a eukaryotic NSS and was proposed as a paradigm for the allosteric action of drugs on NSS function (17).

MhsT was crystallized in an inward-facing conformation with Na^+ in both the Na1 and Na2 sites and a single substrate

Significance

The crystal structure of the human serotonin transporter (hSERT) features a drug bound not only in the primary site, but also simultaneously in a second site, thereby supporting the existence of two binding sites in neurotransmitter:sodium symporters (NSSs) as we demonstrated previously for the bacterial NSS homolog LeuT. Here, we provide evidence that MhsT, another NSS homolog, can simultaneously bind substrate molecules both in its primary substrate (S1) site and in its secondary substrate (S2) site. As in LeuT, substrate binding to both the S1 and S2 sites of MhsT is critical for transport, providing further support for a mechanistic model in which the allosteric interaction between the two substrate sites is a key element of Na^+-coupled symport.

Author contributions: M.Q., L.S., and J.A.J. designed research; M.Q., A.M.A., P.W., and L.S. performed research; M.Q., A.M.A., L.S., and J.A.J. analyzed data; and M.Q., H.W., L.S., and J.A.J. wrote the paper.

The authors declare no conflict of interest.

This article is a PNAS Direct Submission.

[1]To whom correspondence may be addressed. Email: mq2102@cumc.columbia.edu or Jonathan.Javitch@nyspi.columbia.edu.

This article contains supporting information online at www.pnas.org/lookup/suppl/doi:10.1073/pnas.1717444115/-/DCSupplemental.

Published online August 6, 2018.

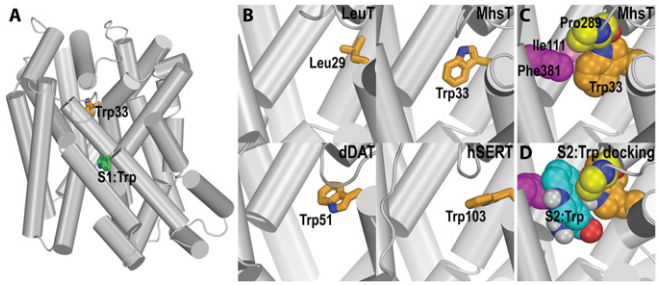

Fig. 1. Dynamics of Trp33 in the extracellular vestibule of MhsT may allow Trp binding in the S2 site. (*A*) Overall scheme of the S1 and S2 sites in MhsT. (*B*) The extracellular vestibules in the crystal structures of LeuT (PDB ID code 2Q6H), MhsT (PDB ID code 4US4), dDAT (PDB ID code 4XP4), and hSERT (PDB ID code 5I6X), showing the variable positioning of the residues aligned to Trp33 of MhsT. (*C*) Trp33 is located at the interface of TM1, TM3, TM10, and EL4, among residues aligned with those that contribute to the previously identified S2 site of LeuT. (*D*) The docking of a Trp molecule in the S2 site, using the induced-fit docking protocol (58) implemented in Schrodinger suites (2014-4). Rotation of the Trp33 side chain in the occluded extracellular vestibule allows the S2 site to accommodate a Trp molecule.

molecule, tryptophan (Trp), bound in the S1 site (PDB ID codes 4US3 and 4US4) (13). Notably, the extracellular vestibule, which contains the S2 site in LeuT, is collapsed in the MhsT structures. A prominent feature of this collapsed extracellular vestibule is the tight packing of Trp33 in transmembrane segment (TM) 1b by hydrophobic residues from extracellular loop (EL) 4, TM3, and TM10, proposed to form the S2 site in LeuT (Fig. 1*A*) (13). This Trp is highly conserved across the NSS family, with LeuT as a notable exception with a Leu at the aligned position (Fig. 1*B*). Our initial studies using scintillation proximity assay (SPA)-based radiolabeled substrate binding showed a substrate-to-protein equilibrium binding stoichiometry of 1 Trp:MhsT in DDM (13), which prompted us to consider a mechanistic hypothesis in which the conserved Trp might act as an "intramolecular S2 substrate" in NSS (other than LeuT) by enabling a mechanism in which its collapse into the S2 site provides the allosteric trigger for inward opening (Fig. 1*C*), in contrast to the binding of an exogenous S2 substrate in LeuT (20). However, we find from computational docking using the MhsT crystal structure that a second Trp molecule can bind in a site functionally homologous to the S2 site of LeuT, with the only adjustment being the rotation of the Trp33 side chain to create space for this S2-bound substrate (Fig. 1*D*).

Thus, to assess whether the two-site transport model we proposed for LeuT also applies to MhsT, we have now pursued radiotracer-based binding and transport assays, as well as cysteine accessibility studies on wild-type (WT) and mutant MhsT constructs. We show that MhsT, like LeuT (20), can simultaneously bind two substrate molecules under equilibrium conditions and that both sites are essential for transport.

Results

Effect of the Detergent on Substrate Binding. Given our previous findings that substrate binding to the S2 site in LeuT is sensitive to both detergent choice and concentration (28, 29), we compared binding to MhsT after solubilization in DDM versus *n*-decyl-β-D-maltopyranoside (DM), a detergent with the same headgroup but a shorter alkyl chain. Presteady-state time points showed that binding of 0.5 μM ^{3}H-Trp, the substrate bound in the MhsT crystal structure (13), to MhsT prepared and assayed in 0.1 (wt/vol)% DDM ($MhsT_{DDM}$) approaches about 50% of that observed for MhsT prepared and assayed in 0.1 (wt/vol)% DM ($MhsT_{DM}$) (Fig. 2*A*). Notably, in contrast to LeuT where substrate binding to the S2 site was sensitive to increasing DDM concentration (29), lowering the DDM concentration during the purification and elution of MhsT to 0.02% [about 2-fold its critical micellar concentration (CMC)] (31) led to binding levels comparable to those observed in 0.1% DDM. Furthermore, raising the DM concentration from 0.1% (slightly above its CMC) (32) to 1.0% (about 10-fold its CMC) did not inhibit binding, as expected if higher concentrations of detergent penetrate the S2 site (*SI Appendix*, Fig. S2) as shown for LeuT (30).

The ^{3}H-Trp saturation binding experiments using equilibrium dialysis (Fig. 2*B*) or SPA-based binding studies (Fig. 2*C*) showed that $MhsT_{DDM}$ exhibits a molar binding stoichiometry of ~1 (*SI Appendix*, Table S1), consistent with our previous measurements (13). Remarkably, however, $MhsT_{DM}$ binds approximately two molecules of Trp under saturating substrate conditions (Fig. 2 *B* and *C* and *SI Appendix*, Table S1). The dissociation constant (K_d) for Trp binding is not substantially affected by the detergent (*SI Appendix*, Table S1). To eliminate altogether the effect of detergent on the interaction of MhsT with its substrate, $MhsT_{DDM}$ and $MhsT_{DM}$ were incorporated into nanodiscs ($MhsT_{ND}$; *SI Appendix*, Fig. S3), artificial ~10 nm-sized phospholipid bilayers

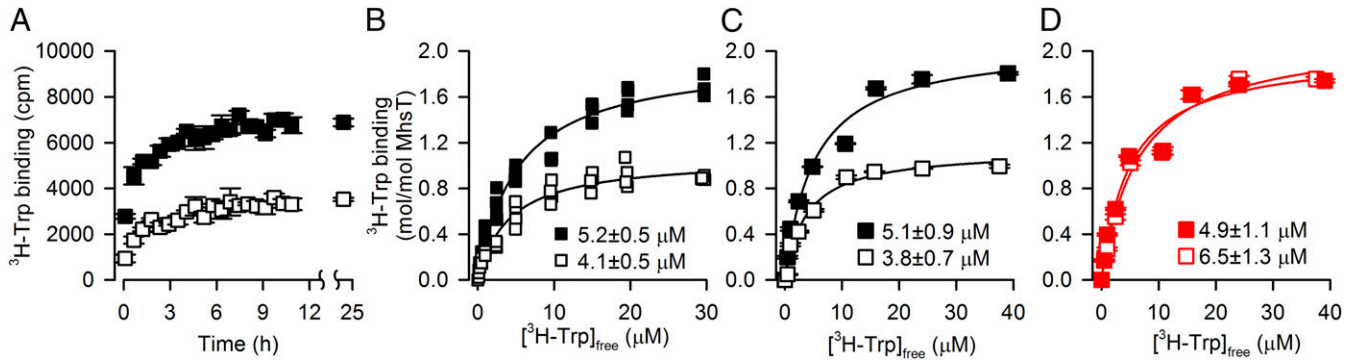

Fig. 2. Binding activity of MhsT in different environments. (*A*) Time course of 0.5 μM ^{3}H-Trp (20 Ci/mmol) binding by $MhsT_{DM}$ (solid square) or $MhsT_{DDM}$ (open square) measured with the SPA. (*B* and *C*) Saturation binding of ^{3}H-Trp by $MhsT_{DM}$ or $MhsT_{DDM}$ performed in NaCl-containing buffer in the presence of DM or DDM, respectively, using equilibrium dialysis (*B*) or the SPA (*C*). (*D*) ^{3}H-Trp saturation binding by MhsT reconstituted into nanodiscs using the SPA. $MhsT_{DM}$ (solid red square) or $MhsT_{DDM}$ (open red square) was inserted into nanodiscs made of polar *E. coli* lipids. Data in *A*, *C*, and *D* are shown as mean ± SEM of triplicate determinations of a representative experiment ($n \geq 3$ with samples from two independent preparations). Data in *B* are from duplicate determinations using protein from two independent preparations and subjected to global fitting using a one-site-specific binding model in Prism 7. The dissociation constants (K_d) of the global fits are shown. The K_ds shown in *C* and *D* were obtained by fitting the data of the representative experiments to a one-site binding model. The kinetic constants of the global fits are summarized in *SI Appendix*, Table S1.

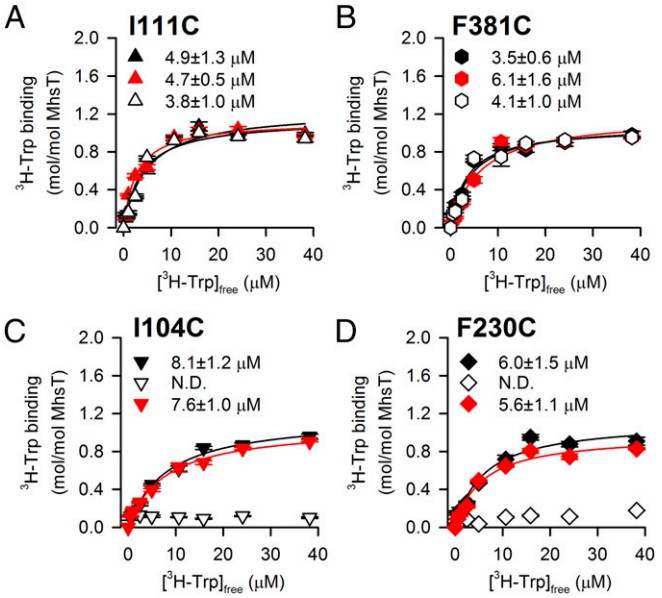

Fig. 3. Binding and transport of MhsT variants. ^{3}H-Trp saturation binding by MhsT-I111C (*A*; triangle), -F381C (*B*; hexagon), -I104C (*C*; inverted triangle), and -F230C (*D*; diamond) was measured with the SPA as described in the legend to Fig. 2. Protein variants solubilized, purified, and assayed in DM are shown as solid symbols, whereas those in DDM are shown as open symbols. Red symbols represent the binding data for variants reconstituted into nanodiscs. Data are shown as mean ± SEM of triplicate determinations of a representative experiment ($n = 3$) and the K_ds shown are based on one-site-specific binding algorithms in Prism 7 of each representative experimental dataset. See *SI Appendix*, Table S1 for a summary of the kinetic constants of the global fits.

encircled by two α-helical membrane scaffold proteins, which have been successfully used as a more native lipid environment for the functional analysis of membrane proteins (22, 33–35). Saturation binding of $MhsT_{ND}$ yielded a B_{max} of ∼2 Trp/MhsT, regardless of whether $MhsT_{DDM}$ or $MhsT_{DM}$ was used for the reconstitution (Fig. 2*D* and *SI Appendix*, Table S1).

Role of S2-Site Residues in Substrate Binding and Transport. As discussed above, docking studies indicate that a Trp substrate molecule can be accommodated in the extracellular vestibule of the MhsT crystal structure in the space freed by rotating the side chain of Trp33 (Fig. 1*D*). The resulting pose places the tryptophan in a potential S2 site with substantial similarity to that in LeuT. To validate the S2 site and characterize its functional importance, we investigated the effects of mutating putative S2 site residues. We selected residues Ile111 and Phe381 in MhsT that align, respectively, with LeuT residues Ile111 and Leu400, both of which are crucial for substrate binding in the S2 site and for substrate transport by LeuT (20, 29). We also selected residues from the S1 site—Ile104 and Phe230 in MhsT that align with Val104 and Phe253 in LeuT—which we have shown to be essential for substrate binding and transport in LeuT (20, 29) and which were seen to interact with the S1 Trp substrate in the MhsT crystal structures (13).

Saturation binding studies were carried out with MhsT variants in which Ile104, Phe230, Ile111, or Phe381 was replaced with Cys and protein purified and assayed in DM or DDM, as well as with these MhsT variants reconstituted into nanodiscs. In DM, all these mutants bind one molecule of Trp with affinities that are similar to that measured for $MhsT\text{-}WT_{DM}$ (Fig. 3 and *SI Appendix*, Table S1). This result indicates that each mutation by itself, in either the S1 or S2 site, reduces the molar binding stoichiometry from 2 observed for $MhsT\text{-}WT_{DM}$ to 1, consistent with disruption of either the S1 or S2 site, and highlights that under equilibrium conditions substrate can bind independently to either site.

In DDM, the S2-site mutants (MhsT-I111C or -F381C) also exhibit a stoichiometry of ∼1 (Fig. 3 *A* and *B* and *SI Appendix*, Table S1), which is expected if DDM's role in reducing the WT stoichiometry to 1 is due to its disrupting the S2 site, since in these constructs this site is already disrupted by the mutations. Consistent with this hypothesis, and in contrast to findings in DM, the S1-site mutants (MhsT-I104C or -F230C) show virtually no binding activity in DDM at the Trp concentrations tested (Fig. 3 *C* and *D* and *SI Appendix*, Table S1). This is consistent with loss of binding to the S1 site through mutation, compounded by loss of binding to the S2 site due to DDM. Reconstitution of the S1- and S2-site MhsT variants into nanodiscs followed by saturation binding measurements mimics the behavior observed for protein prepared and assayed in DM (Fig. 3 and *SI Appendix*, Table S1). These results are consistent with the S2 site being intact in both DM and lipid, but impaired in DDM.

To test the effect of the S1- or S2-site mutations on active transport of Trp, we measured ^{3}H-Trp uptake in intact *Escherichia coli* cells expressing the individual MhsT variants (*SI Appendix*, Fig. S4). Mutation of key positions in either the S1 or S2 sites of MhsT resulted in an activity pattern for MhsT-I104C, -I111C, -F230C, or -F381C that is virtually indistinguishable from that observed for control cells lacking MhsT, highlighting the importance of the integrity of both the S1 and S2 substrate sites for substrate transport in MhsT, just as in LeuT (20).

The Conserved Trp33 Is Not Essential for MhsT Function. Given our findings that a second Trp can bind in the S2 site, we sought to better understand the role of the highly conserved Trp33. Notably, we have recently shown in MhsT that the packing of Trp33 and its nearby residues in the extracellular vestibule is affected by the binding and dissociation of Na2, and this effect is propagated through reconfiguration of an aromatic cluster in TM3 and TM6, in a manner that allosterically couples this region to conformational changes on the intracellular side of the transporter (36). To test the functional importance of Trp33 in MhsT, we introduced Cys, Ala, or Leu at this position and tested the effect of the mutations on binding and transport activity.

Fig. 4*A* shows saturation binding of ^{3}H-Trp by MhsT-W33A, -W33C, and -W33L in the presence of DM. In contrast to MhsT-WT, where the binding isotherm fits a single-site binding model (Fig. 2*C*), the saturation binding data of the three Trp33 mutants did not fit well to a single-site model but instead to a single-site model with variable Hill slope (F test, $P < 0.001$ for all three mutants), which yielded molar binding ratios of ∼2, K_ds of ∼7 μM, and Hill coefficients between 1.7 and 2.0 (*SI Appendix*, Table S1).

Consistent with only small changes in substrate binding to the S1 and S2 sites, all three mutants showed substantial transport activity (Fig. 4*B*). Analysis of the uptake kinetics (*SI Appendix*, Fig. S5*A* and Table S1) showed that the maximal velocity of transport (V_{max}) of the mutants relative to MhsT-WT is between ∼30% (MhsT-W33A or -W33L) and ∼40% (MhsT-W33C). The concentration of Trp yielding half-maximum transport velocity (K_m, about 1 μM for MhsT-WT) was only slightly altered by the mutations (*SI Appendix*, Table S1). These results suggest that while the Trp33 side chain likely plays some role in the transport mechanism, it is not essential for transport, in contrast to the S2-site residues Ile111 and Phe381, mutation of which ablates transport (*SI Appendix*, Fig. S4*A*).

Proximity of the Trp33 Locus to the S2 Site Revealed with the Substituted-Cysteine Accessibility Method. Taking advantage of the fact that MhsT has no native Cys, we were able to explore the involvement of the Trp33 locus in binding and transport using the substituted-cysteine accessibility method (SCAM) (37). To

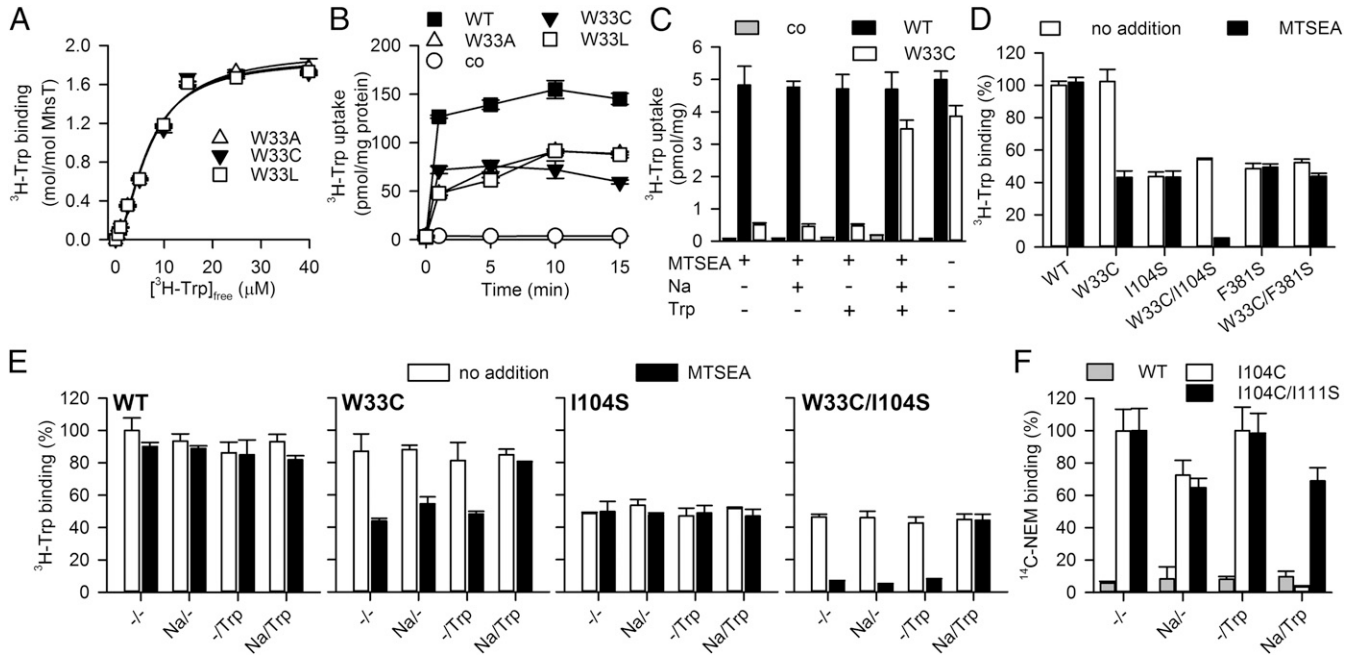

Fig. 4. Functional importance of Trp33 in MhsT. (*A*) Saturation binding of ^{3}H-Trp by the MhsT variants W33A (△), W33C (▼), and W33L (□). Data (mean ± SEM of triplicate determination of a representative experiment, $n = 3$) were fit to the Hill equation (see text for details). (*B*) Time course of 0.1 μM ^{3}H-Trp uptake in *E. coli* MQ614 expressing MhsT-WT (■), -W33A (△), -W33C (▼), or -W33L (□). MQ614 transformed with plasmid pQE60 (○) served as control. Uptake was measured in 10 mM Tris/Mes, pH 8.5/50 mM NaCl. (*C*) Effect of MTSEA on the transport of 0.1 μM ^{3}H-Trp during the initial 30-s period. Cells of MQ614 harboring MhsT-WT (black bar), -W33C (white bar), or a control plasmid (gray bar) were incubated in the presence or absence of 0.5 mM MTSEA in the presence or absence of 50 mM NaCl and/or 50 μM Trp for 20 min before uptake measurements. (*D*) Effect of MTSEA on 0.5 μM ^{3}H-Trp binding by indicated MhsT variants. (*E*) Substrate-specific protection of the engineered thiol group at position 33 in MhsT. SPA-based binding of 0.5 μM ^{3}H-Trp was performed after preincubation of MhsT-WT, -W33C, -I104S, or -W33C/I104S with or without 0.5 mM MTSEA in the presence or absence of 50 mM NaCl and/or 50 μM Trp. (*F*) Substrate binding to the S2 site protects the single Cys at position 104 from interaction with ^{14}C-NEM. Reaction of 20 μM ^{14}C-NEM by MhsT-I104C (containing a thiol side chain in the S1 site; open bars) or by MhsT-I104C/I111S (featuring a single Cys at position 104 and an impaired S2 site by the I111S mutation; solid bars) was measured in the presence or absence of 150 mM NaCl and/or 20 μM Trp. MhsT-WT (devoid of native Cys) served as control. SPA-based ^{14}C-NEM binding was assayed with 100 ng of protein purified in DM in 200 mM Tris/Mes (–/–), 200 mM Tris/Mes plus 20 μM Trp (–/Trp), 50 mM Tris/Mes plus 150 mM NaCl (Na/–), or 50 mM Tris/Mes plus 150 mM NaCl and 20 μM Trp (Na/Trp). Data in *A*–*E* are mean ± SEM of triplicate determinations of a representative experiment ($n \geq 3$); data in *F* are the mean ± SEM of four independent experiments of technical triplicates.

this end, we used the functional MhsT-W33C mutant (which displays only slightly impaired initial rates of transport compared with MhsT-WT; Fig. 4*B* and *SI Appendix*, Fig. S5*A* and Table S1), and the positively charged methanethiosulfonate ethylammonium (MTSEA), a sulfhydryl-specific reagent that reacts readily with water-accessible Cys (37). MTSEA did not affect background uptake activity in control cells lacking MhsT, and, as expected given the absence of Cys in MhsT-WT, preincubation of cells expressing MhsT-WT with MTSEA had no effect on the initial rate of ^{3}H-Trp uptake (Fig. 4*C*). In contrast, MTSEA pretreatment of MhsT-W33C reduced uptake to ∼12% of that observed for the same mutant in the absence of MTSEA. Thus, although the Trp33 side chain tolerates mutation to Cys, chemical modification of the sulfhydryl by MTSEA, which results in a Lys-like side chain, greatly disrupts transport. Remarkably, when the preincubation was performed in the presence of both Na^{+} and Trp, the activity of MTSEA-treated MhsT-W33C was 90 ± 7% of that observed for the nontreated mutant (Fig. 4*C*), revealing a protective effect of Na^{+} and Trp, the two cotransported substrates of MhsT. In contrast, neither Na^{+} alone nor Trp alone afforded protection of the thiol group located in the S2 site against MTSEA (Fig. 4*C*).

To confirm that the effect of MTSEA reaction with the engineered Cys at position 33 is due to disruption of the S2 site, we performed SPA-based ^{3}H-Trp binding experiments in the presence or absence of MTSEA with purified, DM-solubilized MhsT-WT, -W33C, as well as -W33C/I104S and -W33C/F381S. Note that like the Cys mutations of Ile104 (S1 site) or Phe381 (S2 site) (Fig. 3), the Ser mutations reduced the binding stoichiometry from 2, as observed in MhsT-WT and -W33C, to 1 (*SI Appendix*, Fig. S5*B*). Incubation of MhsT-W33C with MTSEA reduced binding by about 50% while it had no effect on the binding activity of MhsT-WT, -I104S, or -F381S (Fig. 4*D*). Combining the W33C mutation with the I104S or F381S mutation yielded constructs (MhsT-W33C/I104S and -W33C/F381S) with binding properties virtually indistinguishable from that of the individual S1 (I104S) or S2 (F381S) mutant (*SI Appendix*, Fig. S5*C*). Notably, MTSEA treatment only marginally reduced the binding activity of MhsT-W33C/F381S, which already has a disrupted S2 site. In contrast, preincubation of MhsT-W33C/I104S with MTSEA reduced the binding activity of that mutant from 54.1 ± 0.9% to 5.6 ± 0.2% of nontreated MhsT-WT (Fig. 4*D*). Since Trp binding in the S1 site of MhsT-W33C/I104S is impaired due to the I104S mutation (*SI Appendix*, Fig. S5*C*), this result indicates that the reaction of MTSEA with Cys at position 33 specifically inhibits substrate binding to the S2 site in MhsT.

Similar to the transport studies (Fig. 4*C*), we found that preincubation of purified MhsT-WT or -I104S with MTSEA had little effect on subsequent ^{3}H-Trp binding activity (Fig. 4*E*). MTSEA reaction with Cys at position 33 in the WT, or I104S background (MhsT-W33C or MhsT-W33C/I104S, respectively), reduced ^{3}H-Trp binding from 100 to ∼50% or from ∼50% to ∼5% of their control values, respectively (Fig. 4*E*). This is consistent with disruption of the S2 site in the context of an intact or a disabled S1 site, respectively. When Na^{+} and Trp were added together during the MTSEA preincubation, the ^{3}H-Trp binding

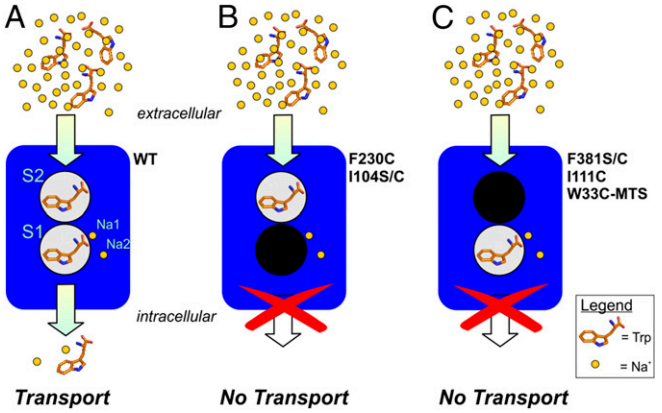

Fig. 5. Schematic representation of the role of the two substrate binding sites in Na^+/substrate symport by MhsT. (*A*) The electrochemical Na^+ concentration gradient across the plasma membrane energizes the translocation of substrate and Na^+. Impairment of (*B*) the S1 site (e.g., by mutation of Phe230 or Ile104) or (*C*) the S2 site (e.g., by mutation of Phe381 or Ile111, or site-directed thiol labeling on the W33C mutant with MTSEA) abolishes transport.

activity was fully protected in both constructs (Fig. 4*E*). Since there is no Trp binding to the S1 site in the I104S mutant, the protection of Cys33 from MTSEA must be mediated through a direct steric effect of substrate Trp bound in the S2 site, and not indirectly by the collapse of the extracellular vestibule in response to S1 binding.

Substrate Binding to the S2 Site Occludes Access to the S1 Site. Having established that Trp binds in the S2 site, we next sought to investigate its impact not just on MTSEA reaction within the S2 site itself, but also on accessibility to the deeper S1 site. To do so in a manner that does not rely on indirect inference of reactivity based upon a functional effect, but rather direct assessment of thiol reactivity, we measured with the SPA the reaction of the thiol-specific reagent ^{14}C-*N*-ethylmaleimide (NEM) to MhsT-I104C, which contains an engineered reporter Cys in the S1 site. Only background ^{14}C-NEM binding was measured in MhsT-WT, consistent with the absence of endogenous Cys (*SI Appendix*, Fig. S6*A*). In contrast, robust ^{14}C-NEM reaction with MhsT-I104C was observed in the absence of Na^+, regardless of whether Trp was present or absent (Fig. 4*F*), consistent with the Na^+ dependence of substrate binding in the S2 site. The ^{14}C-NEM reaction was reduced by ∼27% in the presence of Na^+ alone, consistent with partial closure of the extracellular vestibule in Na^+ (38) slowing access to 104C. In marked contrast, ^{14}C-NEM binding was reduced to background levels when both Na^+ and Trp were present throughout the incubation (Fig. 4*F*), consistent with Trp binding at the S2 site sterically occluding access to the deeper S1 site and thereby protecting the S1 reporter Cys from reaction. When the same set of experiments were carried out with MhsT-I104C/I111S, which has an impaired S2 site due to the I111S mutation (*SI Appendix*, Table S1), the addition of Trp and Na^+ failed to inhibit the NEM reaction with the thiol group at position 104, consistent with the inability of Trp to bind the S2 site (Fig. 4*F*). As expected, the partial protective effect of Na^+ was preserved, since the Na1 and Na2 sites are unaffected by the I111S mutation.

Since the rotamer position of the Phe230 side chain may play an important role in modulating access to the S1 site, as it does for the aligned Phe253 in LeuT (20), we sought to determine whether S2-mediated protection of 104C results from rearrangement of the Phe230 side chain or whether sterically blocking the pathway from the extracellular vestibule to 104C is sufficient, in which case protection should not depend on the Phe230 side chain. The I104C/F230A double mutant showed a virtually identical pattern of Trp protection as observed for MhsT-I104C alone (*SI Appendix*, Fig. S6*A*), most consistent with steric block of the pathway to the S1 site by substrate bound in the S2 site.

Discussion

Our initial studies showing a Trp:MhsT stoichiometry of 1 in DDM (13) prompted us to consider a mechanism in which the conserved Trp in the extracellular vestibule (Trp33 in MhsT) might take the place of an exogenous S2 substrate in NSS family members other than LeuT. Accordingly, the collapse of this Trp into the S2 site could provide an intramolecular allosteric trigger for inward opening that is provided in LeuT by an exogenous S2 ligand. However, we found in subsequent docking studies that the MhsT structure is in fact capable of accommodating a second Trp substrate in a site homologous to the S2 site from LeuT, with the only adjustment being the rotation of the Trp33 side chain (Fig. 1*D*). Here we report that MhsT, like LeuT, can simultaneously bind two substrate molecules per transporter molecule. Mutagenesis analysis verified that residues aligned with those that disrupt S1 or S2 binding in LeuT do the same in MhsT. Furthermore, mutation of any one of these four critical residues abolishes all active transport in MhsT, as it did in LeuT, consistent with the mechanism for transport that we proposed previously in which binding of the S2 substrate acts allosterically as a "symport effector" to enhance inward opening and release of S1 and Na1 to the cytoplasm (20, 21, 29). Although this mechanism requires substrate binding to both the S1 and S2 sites, flux studies using radiolabeled Na^+ and substrate in the related NSS member GAT [the γ-aminobutyric acid (GABA) transporter] suggest a net transport of two Na^+ and one substrate molecule per reaction cycle (10). Notably, although this transport stoichiometry has not been measured in any other NSS, most likely only one substrate molecule (S1) is transported per cycle, along with cotransport (or symport) of two Na^+ (Fig. 5).

It is now apparent that all of the LeuT structures with ligand in the S1 site contain density in or near the S2 site that is either OG, the TCAs clomipramine or imipramine, the SSRI paroxetine, the inhibitor tryptophan, or a still unidentified molecule (11, 25–28, 39–42) (*SI Appendix*, Fig. S1). In the recent hSERT crystal structure with S-citalopram, ligand was identified not only in the S1 site but also in a second site in the extracellular vestibule (17). There is no doubt, therefore, that the S2 site can bind small-molecule ligands, and we agree with the statement in Coleman et al. (17) regarding this second binding site (termed there "allosteric site"): "The malleability of the allosteric site opens the possibility that, depending on the shape and size of the allosteric ligand, occupancy of the allosteric site might not necessarily abrogate transport activity. Indeed, it is conceivable that there could be a spectrum of small molecules that range from inhibiting to enhancing transport activity." This is consistent with our data in LeuT and now MhsT and the allosteric role that a substrate bound in the S2 site has in enabling transport activity (20, 43).

Nonetheless, the questions of whether substrate binds in the S2 site, and if so, whether this is an atypical property of LeuT that is not shared by other NSS members, have remained contentious. The first reservation that has been raised is that substrate has not been crystallized in the S2 site. If the S2 site in LeuT can be crystallized with detergent, TCAs, SSRIs, and the inhibitor amino acid Trp, one might expect that it could be crystallized with Leu. However, extensive efforts by multiple laboratories including our own have failed to yield a structure with substrate in the S2 site. This "failure" is consistent with our biochemical (20), biophysical (21), and computational (20, 21) data suggesting that substrate binding in the S2 site of LeuT

allosterically triggers inward opening of the transporter and thus enhances dynamics that would be expected to impair crystallization (21).

The second argument against the S2 site binding substrate in LeuT was a study that measured the stoichiometry as 1 (23) in contrast to our measurements of 2 (20, 28, 29). However, we were able to replicate these results, reducing the stoichiometry from 2 to 1 by raising the concentration of DDM (29), in accordance with the published studies. We found that elevated DDM concentration irreversibly blocked binding to the S2 site in LeuT, an effect that could only be undone by removal of the detergent during reconstitution into liposomes (29). An independent study also has measured the stoichiometry in nanodiscs to be ~2 (22). A recent study that used NMR to measure stoichiometry was a technical tour de force, but unfortunately failed to use more routine binding measurements to characterize the protein used in the NMR experiments and determine whether the S2 site was in fact intact after detergent treatment, and thus is, unfortunately, not helpful in clarifying the native stoichiometry (24).

Although a preponderance of evidence now suggests that the stoichiometry of LeuT is in fact 2, and that substrate binding to the S2 site allosterically plays a critical role in inward opening and the transport cycle (43), it had remained an important open question as to whether this mechanism is limited to LeuT. Here we extend this mechanism to MhsT. As mentioned above, we focused our studies on Trp33, which is located in the collapsed extracellular vestibule of MhsT (Fig. 1*B*). In comprehensive sequence alignments of NSSs compiled for our previous study (44) that includes both eukaryotic and prokaryotic members, this position is a Trp in all of the eukaryotic NSS sequences retrieved from the Swiss-Prot database, and in all prokaryotic NSS sequences retrieved from RefSeq database, with the only exceptions being LeuT (Leu29) and three other transporters from uncharacterized thermophilic *Pyrococcus* species (all Val). In hDAT, mutation of the aligned Trp84 enhanced cocaine binding, consistent with a more outward-open configuration, and reduced transport by slowing inward release of dopamine (45, 46). The corresponding W68L mutation in GAT1 also markedly reduced transport due to increased Na^+ affinity and impaired substrate release (47). These results are consistent with a role for this conserved Trp in enhancing the transition to the inward-facing conformation, just as we inferred for S2 binding in LeuT (21).

Since MhsT has a rate of transport quite similar to that of the human biogenic amine transporters (13), it serves as a much better model for these clinically relevant targets in which to answer the question of whether the binding of a substrate triggers the S2 allosteric mechanism or whether the intramolecular collapse of the conserved Trp into the S2 site serves this role. In MhsT, we have shown that mutation of Trp33 is readily tolerated, as the binding stoichiometry remains 2 and uptake is only modestly reduced. Nonetheless, a more radical "mutation," created by reacting MTSEA with an engineered Cys at this position disrupts S2 binding and inhibits transport, demonstrating the functional involvement of this locus. Notably, the reaction of MTSEA with this Cys can be protected against by the substrate Trp (only in the presence of Na^+, which is needed for binding). We showed here that this protection does not result from a conformational change associated with binding of Trp to the S1 site but in fact results from direct steric block within the S2 site, as protection was preserved in a substrate binding-deficient S1-site mutant. This establishes that Trp33 is near the critical S2 site.

We also showed that binding of Trp to the S2 site protects an engineered Cys in the S1 site, presumably by blocking access deeper into the transporter (*SI Appendix*, Fig. S6*B*). Indeed, our computational analysis indicates that the presence of substrate Trp in the S2 site maintains the extracellular vestibule in a collapsed state, which is expected to restrict the bulky NEM molecule from accessing the S1 site, consistent with the observed reduction in S1 accessibility in the presence of S2-bound substrate. Note that in the absence of substrate, the transporter is expected to be in an outward-facing conformation with the S1 site exposed to the water milieu (48, 49). We rule out that Trp binding in the mutated S1 site of the MhsT-I104C mutant can compete with NEM as saturation binding reveals only occupation of the S2 site in this mutant at the Trp concentration (20 μM) chosen for the NEM labeling experiment.

In addition to LeuT and MhsT, the two-substrate stoichiometry demonstrated here is also shared with other LeuT-fold transporters without primary sequence homology to LeuT, namely PutP and vSGLT, in which the substrate stoichiometry has also been shown to be 2 and in which mutation of residues in the presumed S2 site abolishes transport (50). Given the structural and functional similarities among NSS members, it seems likely that the two-substrate model will also extend to eukaryotic NSSs, although this must be explored experimentally. Of note, mutation of the conserved Trp in GAT severely disrupted transport, consistent with the possibility of a more important role for this side chain in eukaryotic proteins. Notably, however, only a moderate impairment of transport was observed in DAT upon mutation of this residue, more similar to the results we presented here for MhsT. These questions must therefore be addressed more directly both computationally and experimentally in eukaryotic NSSs. Such studies cannot be limited to assessing the stability of a substrate bound in S2 for the length of a molecular dynamics (MD) trajectory, but must include a quantitative model of the manner in which the binding of a second substrate is connected to functional mechanisms such as allosteric coupling to inward opening. Allosteric propagation mechanisms that have been elaborated and applied to NSS proteins (e.g., see refs. 20, 36, 43, and 51–54) have been based on extensive MD simulations in combination with Markov state model (MSM) analysis. The predictions from such studies, probed with specific binding and flux experiments, will further reveal the nature and role of the S2 site in the function of MhsT and cognate NSS family members.

Materials and Methods

Gene Expression, Protein Purification. The *mhsT* WT gene or mutated versions of *mhsT* (flanked by a sequence that encodes an N-terminal 10×His tag and TEV protease cleavage site) were expressed from a pNZ8048 derivative in *Lactococcus lactis* NZ9000 (12). PCR-based site-directed mutagenesis was used to replace Trp33, Ile104, Ile111, Phe230, and Phe381 in individual fashion and double mutants were generated by swapping mutagenized fragments using appropriate restriction sites. The fidelity of the resulting *mhsT* variants was confirmed with sequencing (Macrogen, Inc.). After solubilization of inverted membrane vesicles of *L. lactis* producing the appropriate MhsT variant with 1.5% (wt/vol) of the detergent used for the subsequent immobilized metal-chelate chromatography (IMAC), protein was purified in 50 mM 2-amino-2-(hydroxymethyl)-1,3-propanediol (Tris)/2-(*N*-morpholino)-ethanesulfonic acid (Mes), pH 7.5/20% glycerol/150 mM NaCl/1 mM Tris(2-carboxyethyl) phosphine (TCEP)/0.1% (wt/vol) DDM or DM as previously described (12, 13). When indicated, the concentration of DDM during IMAC was reduced to 0.02%. HPLC-mediated size-exclusion chromatography (on a Shodex Protein-KW803 column) was used for buffer exchange. Immediately before the size-exclusion chromatography the protein was concentrated using centrifugal filtration with Vivaspin6, molecular weight cutoff (MWCO) 50,000 devices.

Reconstitution of MhsT-Containing Nanodiscs. MSP1E3D1 and lipids were prepared as described (35). *E. coli* polar lipids (Avanti) were dissolved in chloroform, dried under a stream of nitrogen gas, and resuspended at a concentration of 20 mM in 10 mM Tris pH 7.4, 100 mM NaCl, 0.5 mM EDTA and 0.01% NaN_3. Nanodiscs were formed at a molar ratio of 0.1 MhsT:1 MSP1E3D1:500 lipids. Detergent was removed by serial addition of Biobeads SM2 (Biorad) and the MhsT nanodiscs were resuspended in 100 mM Tris/Mes, pH 7.4/1 mM TCEP after ultracentrifugation of the samples at 365,000 × *g* for 1 h. The protein concentration of all samples was measured with the Amidoblack protein assay (55) and, in addition, the concentration of MhsT in nanodiscs was quantified from silver-stained SDS/PAGE gels with densitometry

using ImageJ (NIH) using known amounts of purified MhsT as reference (*SI Appendix*, Fig. S3).

Transport Assay. Transport of L-[^{3}H]tryptophan (American Radiolabeled Chemicals, Inc) was measured in intact *E. coli* MQ614 harboring pQE60 (serving as control) or pQE60 derivatives containing the appropriate *mhsT* variants (that, in analogy to the pNZ8048 derivatives mentioned above, encode an N-terminal His tag and TEV site) as described (13, 56). To assess the relative amounts of the MhsT variants in the membrane of the *E. coli* cells, membrane vesicles were produced from MQ614 cells expressing the given *mhsT* variants or those transformed with pQE60 (no *mhsT*). Normalized amounts (10 μg of total membrane protein) of the membrane vesicles were subjected to SDS/PAGE followed by immunoblot analysis using His probe (Santa Cruz Biotechnology, Inc.) and a horseradish peroxidase-based chemiluminescence detection method (SuperSignal West Pico kit; Thermo Scientific).

Binding Studies. L-[^{3}H]tryptophan binding to purified MhsT variants was performed in 50 mM Tris/Mes, pH 7.5/20% glycerol/150 mM NaCl/1 mM TCEP/0.1% DM or DDM as indicated. To test the effect of the detergent concentration on the MhsT binding activity (*SI Appendix*, Fig. S2), the DM and DDM concentrations were varied. Equilibrium dialysis was carried out with the HTD96b dialysis 96-well apparatus and 12,000–14,000 MWCO membranes using 500 ng of purified protein as described (29). For SPA-based binding studies, 50 ng of protein was bound to 250 μg of Cu^{2+}-coated yttrium silicate (YSi) SPA beads in an assay volume of 100 μL. Binding studies using MhsT reconstituted in nanodiscs were performed with the SPA in 50 mM Tris/Mes, pH 7.5/150 mM NaCl/1 mM TCEP and 50 ng of protein per assay. ^{3}H-Trp binding with the SPA was performed in the dark for 16 h at 4 °C with vigorous shaking on a vibrating platform.

Reactivity of 20 μM ^{14}C-NEM (55 mCi/mmol) with the engineered Cys at position 104 (MhsT-I104C) was measured with the SPA and 100 ng of indicated DM-purified MhsT variants in 50 (or 200) mM Tris/Mes, pH 7.5/150 (or 0) mM NaCl/20% glycerol/0.1 mM TCEP/0.1% DM in the presence or absence of 20 μM Trp as indicated. Reactions were performed in the dark for 5–30 min at 4 °C. All SPA samples were counted in the SPA mode of a Wallac 1450 MicroBeta plate PMT counter. A total of 800 mM imidazole (which prevents the interaction of the His-tagged protein with the Cu^{2+}-coated SPA beads) was added to the samples to determine the nonproximity background signal. All SPA-based experiments were performed at least in duplicate with replicas of three or more, and data are expressed as mean ± SEM. Equilibrium dialysis was measured in duplicate with protein from two independent preparations. Data fits of kinetic analyses were performed using nonlinear regression algorithms in Prism 7 (GraphPad), and errors represent the SEM of the fit.

Chemical Modification of Cys33. Transport of L-[^{3}H]tryptophan in intact *E. coli* MQ614 expressing MhsT variants that contained a single cysteine in place of Trp33 was measured after the chemical modification of the thiol group of MhsT-W33C with MTSEA (kindly provided by A. Karlin, Columbia University, New York) (57) in the presence or absence of ligands. Briefly, before uptake measurements, cells expressing MhsT-WT, -W33C, or -W33C in combination with the S1-site mutant I104S or the S2-site mutant F381S were incubated with 0.5 mM MTSEA for 20 min at 23 °C in the presence or absence of 50 mM NaCl and/or 50 μM Trp in 100 mM Tris/Mes, pH 7.5. *E. coli* MQ614/pQE60 served as control. Cell suspensions were washed with the reaction buffer lacking MTSEA followed by three washes with 100 mM Tris/Mes, pH 7.5 before being used for uptake studies.

Data Analysis. Experimental data in figure panels (except those in Fig. 2*B*) are from representative experiments shown as mean ± SEM of triplicate determinations and the corresponding kinetic constants are for the same dataset with the mean ± SEM of the fit. To determine the kinetic constants from independent experiments, individual data of two or more independent binding or transport experiments (with technical triplicates) were subjected to global fitting in GraphPad Prism 7 and the kinetic constants are summarized in *SI Appendix*, Table S1 as mean ± SEM of the global fit. Binding data were fit to a one-site-specific binding model or a specific binding with Hill slope model as determined with the extra sum-of-square *F* test, whereas transport data were fit to the Michaelis–Menten model.

ACKNOWLEDGMENTS. We thank Ashley Lee, Trang Nguyen, and Audrey Warren for technical assistance. This research was supported by NIH Grants U54 GM087519, R01 DA041510 (to J.A.J.), and P01 DA012408 (to H.W.), and by the Intramural Research Program of National Institutes of Health, National Institute on Drug Abuse (A.M.A. and L.S.).

1. Rudnick G, ed (2002) *Mechanisms of Biogenic Amine Neurotransmitter Ttransporters* (Humana Press Inc., Totowa, NJ), 2 Ed, pp 25–52.
2. Sonders MS, Quick M, Javitch JA (2005) How did the neurotransmitter cross the bilayer? A closer view. *Curr Opin Neurobiol* 15:296–304.
3. Hahn MK, Blakely RD (2002) Monoamine transporter gene structure and polymorphisms in relation to psychiatric and other complex disorders. *Pharmacogenomics J* 2: 217–235.
4. Sutcliffe JS, et al. (2005) Allelic heterogeneity at the serotonin transporter locus (SLC6A4) confers susceptibility to autism and rigid-compulsive behaviors. *Am J Hum Genet* 77:265–279.
5. Rothman RB, Baumann MH (2003) Monoamine transporters and psychostimulant drugs. *Eur J Pharmacol* 479:23–40.
6. Butler SG, Meegan MJ (2008) Recent developments in the design of anti-depressive therapies: Targeting the serotonin transporter. *Curr Med Chem* 15:1737–1761.
7. Kanner BI (1978) Active transport of gamma-aminobutyric acid by membrane vesicles isolated from rat brain. *Biochemistry* 17:1207–1211.
8. Gu H, Wall SC, Rudnick G (1994) Stable expression of biogenic amine transporters reveals differences in inhibitor sensitivity, kinetics, and ion dependence. *J Biol Chem* 269:7124–7130.
9. Torres GE, Gainetdinov RR, Caron MG (2003) Plasma membrane monoamine transporters: Structure, regulation and function. *Nat Rev Neurosci* 4:13–25.
10. Krause S, Schwarz W (2005) Identification and selective inhibition of the channel mode of the neuronal GABA transporter 1. *Mol Pharmacol* 68:1728–1735.
11. Yamashita A, Singh SK, Kawate T, Jin Y, Gouaux E (2005) Crystal structure of a bacterial homologue of Na^+/Cl^--dependent neurotransmitter transporters. *Nature* 437: 215–223.
12. Quick M, Javitch JA (2007) Monitoring the function of membrane transport proteins in detergent-solubilized form. *Proc Natl Acad Sci USA* 104:3603–3608.
13. Malinauskaite L, et al. (2014) A mechanism for intracellular release of Na^+ by neurotransmitter/sodium symporters. *Nat Struct Mol Biol* 21:1006–1012.
14. Penmatsa A, Wang KH, Gouaux E (2013) X-ray structure of dopamine transporter elucidates antidepressant mechanism. *Nature* 503:85–90.
15. Wang KH, Penmatsa A, Gouaux E (2015) Neurotransmitter and psychostimulant recognition by the dopamine transporter. *Nature* 521:322–327.
16. Penmatsa A, Wang KH, Gouaux E (2015) X-ray structures of *Drosophila* dopamine transporter in complex with nisoxetine and reboxetine. *Nat Struct Mol Biol* 22: 506–508.
17. Coleman JA, Green EM, Gouaux E (2016) X-ray structures and mechanism of the human serotonin transporter. *Nature* 532:334–339.
18. Abramson J, Wright EM (2009) Structure and function of $Na^{(+)}$-symporters with inverted repeats. *Curr Opin Struct Biol* 19:425–432.
19. Shi L, Weinstein H (2010) Conformational rearrangements to the intracellular open states of the LeuT and ApcT transporters are modulated by common mechanisms. *Biophys J* 99:L103–L105.
20. Shi L, Quick M, Zhao Y, Weinstein H, Javitch JA (2008) The mechanism of a neurotransmitter:sodium symporter–Inward release of Na^+ and substrate is triggered by substrate in a second binding site. *Mol Cell* 30:667–677.
21. Zhao Y, et al. (2011) Substrate-modulated gating dynamics in a Na^+-coupled neurotransmitter transporter homologue. *Nature* 474:109–113.
22. Nasr ML, Singh SK (2014) Radioligand binding to nanodisc-reconstituted membrane transporters assessed by the scintillation proximity assay. *Biochemistry* 53:4–6.
23. Piscitelli CL, Krishnamurthy H, Gouaux E (2010) Neurotransmitter/sodium symporter orthologue LeuT has a single high-affinity substrate site. *Nature* 468:1129–1132.
24. Erlendsson S, et al. (2017) Direct assessment of substrate binding to the neurotransmitter:sodium symporter LeuT by solid state NMR. *eLife* 6:e19314.
25. Singh SK, Yamashita A, Gouaux E (2007) Antidepressant binding site in a bacterial homologue of neurotransmitter transporters. *Nature* 448:952–956.
26. Zhou Z, et al. (2007) LeuT-desipramine structure reveals how antidepressants block neurotransmitter reuptake. *Science* 317:1390–1393.
27. Zhou Z, et al. (2009) Antidepressant specificity of serotonin transporter suggested by three LeuT-SSRI structures. *Nat Struct Mol Biol* 16:652–657.
28. Quick M, et al. (2009) Binding of an octylglucoside detergent molecule in the second substrate (S2) site of LeuT establishes an inhibitor-bound conformation. *Proc Natl Acad Sci USA* 106:5563–5568.
29. Quick M, Shi L, Zehnpfennig B, Weinstein H, Javitch JA (2012) Experimental conditions can obscure the second high-affinity site in LeuT. *Nat Struct Mol Biol* 19:207–211.
30. Khelashvili G, et al. (2013) The membrane protein LeuT in micellar systems: Aggregation dynamics and detergent binding to the S2 site. *J Am Chem Soc* 135: 14266–14275.
31. VanAken T, Foxall-VanAken S, Castleman S, Ferguson-Miller S (1986) Alkyl glycoside detergents: Synthesis and applications to the study of membrane proteins. *Methods Enzymol* 125:27–35.
32. Alpes H, Apell HJ, Knoll G, Plattner H, Riek R (1988) Reconstitution of Na^+/K^+-ATPase into phosphatidylcholine vesicles by dialysis of nonionic alkyl maltoside detergents. *Biochim Biophys Acta* 946:379–388.
33. Whorton MR, et al. (2007) A monomeric G protein-coupled receptor isolated in a high-density lipoprotein particle efficiently activates its G protein. *Proc Natl Acad Sci USA* 104:7682–7687.

34. Ritchie TK, et al. (2009) Chapter 11–Reconstitution of membrane proteins in phospholipid bilayer nanodiscs. *Methods Enzymol* 464:211–231.
35. Zehnpfennig B, Wiriyasermkul P, Carlson DA, Quick M (2015) Interaction of α-lipoic acid with the human Na^+/multivitamin transporter (hSMVT). *J Biol Chem* 290: 16372–16382.
36. Stolzenberg S, et al. (2017) The role of transmembrane segment 5 (TM5) in Na2 release and the conformational transition of neurotransmitter:sodium symporters toward the inward-open state. *J Biol Chem* 292:7372–7384.
37. Karlin A, Akabas MH (1998) Substituted-cysteine accessibility method. *Methods Enzymol* 293:123–145.
38. Terry DS, et al. (2018) A partially-open inward-facing intermediate conformation of LeuT is associated with Na^+ release and substrate transport. *Nat Commun* 9:230.
39. Singh SK, Piscitelli CL, Yamashita A, Gouaux E (2008) A competitive inhibitor traps LeuT in an open-to-out conformation. *Science* 322:1655–1661.
40. Nyola A, et al. (2010) Substrate and drug binding sites in LeuT. *Curr Opin Struct Biol* 20:415–422.
41. Piscitelli CL, Gouaux E (2012) Insights into transport mechanism from LeuT engineered to transport tryptophan. *EMBO J* 31:228–235.
42. Kantcheva AK, et al. (2013) Chloride binding site of neurotransmitter sodium symporters. *Proc Natl Acad Sci USA* 110:8489–8494.
43. LeVine MV, Cuendet MA, Khelashvili G, Weinstein H (2016) Allosteric mechanisms of molecular machines at the membrane: Transport by sodium-coupled symporters. *Chem Rev* 116:6552–6587.
44. Beuming T, Shi L, Javitch JA, Weinstein H (2006) A comprehensive structure-based alignment of prokaryotic and eukaryotic neurotransmitter/Na^+ symporters (NSS) aids in the use of the LeuT structure to probe NSS structure and function. *Mol Pharmacol* 70:1630–1642.
45. Chen N, Zhen J, Reith ME (2004) Mutation of Trp84 and Asp313 of the dopamine transporter reveals similar mode of binding interaction for GBR12909 and benztropine as opposed to cocaine. *J Neurochem* 89:853–864.
46. Lin Z, Wang W, Uhl GR (2000) Dopamine transporter tryptophan mutants highlight candidate dopamine- and cocaine-selective domains. *Mol Pharmacol* 58:1581–1592.
47. Mager S, et al. (1996) Ion binding and permeation at the GABA transporter GAT1. *J Neurosci* 16:5405–5414.
48. Claxton DP, et al. (2010) Ion/substrate-dependent conformational dynamics of a bacterial homolog of neurotransmitter:sodium symporters. *Nat Struct Mol Biol* 17: 822–829.
49. Krishnamurthy H, Gouaux E (2012) X-ray structures of LeuT in substrate-free outward-open and apo inward-open states. *Nature* 481:469–474.
50. Li Z, et al. (2015) Identification of a second substrate-binding site in solute-sodium symporters. *J Biol Chem* 290:127–141.
51. LeVine MV, Weinstein H (2014) NbIT–A new information theory-based analysis of allosteric mechanisms reveals residues that underlie function in the leucine transporter LeuT. *PLoS Comput Biol* 10:e1003603.
52. Khelashvili G, et al. (2015) Computational modeling of the N-terminus of the human dopamine transporter and its interaction with PIP2 -containing membranes. *Proteins* 83:952–969.
53. Billesbølle CB, et al. (2015) Substrate-induced unlocking of the inner gate determines the catalytic efficiency of a neurotransmitter:sodium symporter. *J Biol Chem* 290: 26725–26738.
54. Stolzenberg S, et al. (2015) Mechanism of the association between Na^+ binding and conformations at the intracellular gate in neurotransmitter:sodium symporters. *J Biol Chem* 290:13992–14003.
55. Schaffner W, Weissmann C (1973) A rapid, sensitive, and specific method for the determination of protein in dilute solution. *Anal Biochem* 56:502–514.
56. Quick M, et al. (2006) State-dependent conformations of the translocation pathway in the tyrosine transporter Tyt1, a novel neurotransmitter:sodium symporter from *Fusobacterium nucleatum*. *J Biol Chem* 281:26444–26454.
57. Stauffer DA, Karlin A (1994) Electrostatic potential of the acetylcholine binding sites in the nicotinic receptor probed by reactions of binding-site cysteines with charged methanethiosulfonates. *Biochemistry* 33:6840–6849.
58. Sherman W, Day T, Jacobson MP, Friesner RA, Farid R (2006) Novel procedure for modeling ligand/receptor induced fit effects. *J Med Chem* 49:534–553.